Dynamics of charge carriers on hexagonal nanoribbons with vacancy defects

Wiliam Ferreira da Cunha*
Quantum Theory Project, University of Florida, Gainesville, Florida 32611-2085, USA

Pedro Henrique de Oliveira Neto
Department of Chemistry, MIT, Cambridge, Massachusetts 02139, USA

Akira Terai
Department of Applied Physics, Osaka City University, Osaka 558-8585, Japan

Geraldo Magela e Silva
Institute of Physics, University of Brasilia, Brasilia 70.919-970, Brazil
(Received 24 March 2016; revised manuscript received 2 June 2016; published 1 July 2016)

We develop a general model to investigate the dynamics of charge carriers in vacancy endowed honeycomb two-dimensional nanolattices. As a fundamental application, results concerning the influence of vacancies placed on different sites of semiconducting armchair graphene nanoribbons (AGNR) over the transport of polarons are presented. It is observed that the positioning of vacancies plays a major role over the scattering of the charge carriers, in the sense that their overall mobility is determined by where the defect is allocated. By considering different structural configurations of the system, the arising polaron can either move freely or be reflected. Therefore, our work provides a phenomenological understanding of the underlying mechanism responsible for the change of conductivity experienced by systems in which structural defects are present, a fact that has been reported for different nanostructures of the same symmetry. Because vacancies are one of the most common kinds of defects and are, in practice, unavoidable, the kind of description proposed in the present paper is crucial to correctly address transport and electronic properties in more realistic electronic devices based on two-dimensional nanolattices.

DOI: 10.1103/PhysRevB.94.014301

I. INTRODUCTION

Low-dimensional solid state nanosystems are composed of nanostructures in which at least one of their dimensions are small when compared to the others. In such structures, electrons and holes present quantized energy levels in the smaller of the directions, but are free to move in the others, as the energy is spanned into the continuum for the extended system. This confinement of the electronic wave function is what typically allows these systems to exhibit very diverse properties when compared to traditional three-dimensional structures, usually well described by conventional condensed matter physics. Recently, such properties have been very well exploited from the technological point of view to give rise to a novel generation of devices and applications whose unique traits arise from the peculiar behavior that charge presents in these systems. As examples of low-dimensional structures with important technological appeal one can cite: conducting polymers, one-dimensional systems currently used in the development of an organic photovoltaic technology [1]; carbon and boron nitride nanotubes, interesting quasi-one-dimensional candidates to gas sensing and arrest [2,3]; two-dimensional transition metal dicalcogen alloys, used in optoelectronics applications and hydrogen catalysis [4]; quasi-two-dimensional high temperature organic superconductors, such as BEDT-TTF [5] and, naturally, graphene nanoribbons [6]. Although very diverse in nature, these systems have in common the fact that their peculiar properties cannot be fully explained but in terms of a many-body effect picture. The main idea of this approach is to realize that electrons cannot be viewed as independent entities, but rather—as they are continuously interacting with other electrons, nuclei, defects, and excitations such as phonons and photons—as collective excitations or quasiparticles [7].

The concept of quasiparticle has since long been employed in solid state physics due to the difficulty to address exactly the many body problem for these systems. Based on the success that quantum field theory previously presented, this new picture has been applied to condensed matter problems with extreme success since the mid 50's. By describing the real interacting particles as approximate noninteracting fictitious entities (the quasiparticles) in the scope of an independent particle approach, Drude and Sommerfeld [8] have presented a very elegant and manageable description for the problem. Depending on the nature of the system as well as its environment and the excitations that act upon it, different quasiparticles—with rather different properties—might take place. Of particular interest to the understanding of the behavior of low-dimensional solid state nanostructures is the interaction between electrons (or holes) and phonon modes. This interaction can create a number of different quasiparticles, one of the most important being the polaron. A polaron is an entity that results from the movement of a charged quasiparticle that polarizes the lattice thus causing structural distortion. It is thus a collective excitation that couples the vibrational modes of the crystal lattice (phonon) with the charge (electron or hole). A polaron is able to respond

*wiliam@unb.br

simultaneously to electric and magnetic field inasmuch as it possesses $\pm 1/2$ spin and $\pm e$ charge [9]. This structure can be spontaneously formed in the lattice or, alternatively, can be induced by the presence of impurities, photoionization, or photoexcitation processes or by stress.

As quasiparticles are known to be the usual charge carrier in low-dimensional solid state structures, a considerable amount of work concerning the dynamics of these excitations in different systems has been performed throughout the years [10,11]. Particularly, the interaction between several quasiparticles [12] and between quasiparticles of different natures [13] in the same lattice has been previously discussed. In one of these early works, for instance, Okuno and Onodera proposed the coexistence of a soliton and a polaron in a single conducting polymer chain by means of a continuum model [14]. The interaction between these quasiparticles was then investigated. More recently, a number of scattering processes between different quasiparticles in conjugated polymers were considered in the scope of modified versions of the SSH model [15]. As reasoned in the previous paragraph, the very nature of a polaron requires a certain level of lattice distortion. Therefore, whenever such a quasiparticle is present, one has to deal with a structural defect. In this sense, the interaction of more than one quasiparticle in a single chain can be viewed as (although should not be restricted to) the interaction between a modified quasiparticle and a lattice distortion.

Indeed, although the last few decades were very prolific as far as the synthesis of low-dimensionality nanomaterials is concerned, methods of creating pristine lattices remain rather restricted [16–19]. As already discussed, the nature of charge carriers in these systems actually prevent this being the case. One thing that was learned, however, is that the presence of defects must be very carefully investigated for it is not only unavoidable but rather gives rise to effects that might enhance or harm the system's performance. For instance, Scuzeria and co-workers conducted an interesting study concerning boron nitride nanotubes as gas sensors. In their work, it was shown that the inclusion of mechanically induced vacancy defects in the lattice lead to the formation and dislocation of dipoles on the structure's walls [20], thus potentially raising its chemical reactivity regarding the capture of gas molecules. The reason for this has to do with the fact that the presence of the vacancy tends to cause a charge redistribution towards raising the concentration of electrons or holes around the defect [21,22]. On the other hand, Stafström has shown that depending on the concentration of vacancies, carbon nanotubes can have their conductivity substantially lowered, due to a high probability of charge carriers scattering in the lattice [23]. His work has shown that the conductivity is modified not only as a function of the vacancy concentration itself but also of its relative positions in the lattice. It was reasoned that different vacancy distributions could give rise to stronger or weaker scattering depending on the structure of the carrier's wave function. Be that as it may, a decrease of conductivity is expected to be undesired for applications such as optics or electronics.

The analysis of these results leads to some important conclusions. First, it is clear that in order to predict whether the presence of defects shall improve or harm the efficiency of the system, it is fundamental to first understand the underlying mechanism of interaction between charges and the defects. Second, we observe that the change of the system's efficiency in opposite directions was mainly due to each application rather than to the nature of the lattice. Both systems described were hexagonal tiling honeycomb nanotubes, but whose unit cells were composed of different atoms. Note, however, that the presence of the defect plays the same roles in both cases: It simultaneously create dipoles (which is good for gas adsorption) and increases the scattering (which is harmful for optics and electronic purposes). Third, one should be interested to investigate if the importance of relative positioning of the defect in the chain (as reported by Stafström) is a general pattern, i.e., if it still plays a role in modifying the interaction between charge and defects in other systems. To summarize these conclusions, it can be said that it is mandatory to perform a thorough investigation on the fundamental aspect regarding the interaction between charge and defects (including the effects of the defect position) for low-dimensional solid state systems with different topological configurations.

We have recently developed a study on the effects of impurity-type defects in armchair graphene nanoribbons [24]. It was shown that these defects strongly affect the dynamics of quasiparticle in these materials, either by trapping the charge carriers or by affecting their stability. Nevertheless, a similar theoretical investigation concerning the effects of structural defects, such as vacancies, had not yet been conducted in these two-dimensional systems. The aforementioned works on vacancies in nanotubes whose atoms are distributed in a honeycomb symmetry (BNNTs and CNTs) encourage us to tackle real two-dimensional systems with the same symmetry. As several examples we can consider boron nitride sheets, germanene, silicene, alloys such as WS_2, MoS_2, WSe_2, and $MoSe_2$, and graphene nanoribbons. In the present paper, we develop a parametric model based on a tight-binding approach with lattice relaxation in a first order expansion to treat the charge carrier dynamics in these systems. Although the results presented here are obtained by using parameters that simulate armchair graphene nanoribbons, the model is general and could, in principle, be re-parameterized to comprise other hexagonal two-dimensional lattices, such as those described. However, taking into consideration that, as in the comparative example between Scuzeria and Stafstrom's works, the results for different species are expected to be qualitatively the same—provided the same symmetry is preserved—we have chosen to adopt a more general and qualitative picture of the interacting process, so that a specific reparametrization for other systems is out of the scope of the present paper.

The choice of presenting results specifically for armchair graphene nanoribbons is due to the fact that these structures are representative examples of flat honeycomb lattice with a huge technological appeal. It is well known that graphene nanoribbons of the armchair chirality present a semiconducting character, which makes it even more interesting from the point of view of applications in electronics. For instance, it is observed some devices built out of GNRs presented high permittivity and low loss in the radio and microwave frequencies, which is a critical feature for miniaturization of electronic components and for their use in antennas and other military applications [25]. GNRs have also been successfully

used as electrode materials for batteries and supercapacitors [26], as well as a substrate to grow polyaniline nanorods with enhanced mechanical properties [27]. These works show, from the experimental point of view, the importance of studying both electronic and structural properties in this kind of system. Nevertheless, no theoretical work has discussed these two features together, i.e., the effects of the presence of vacancies as well as of their positioning on the lattice, over the transport properties that provide interesting features to GNRs. Therefore, besides presenting a general qualitative discussion over the role vacancies defects play on the electronic transport in two-dimensional honeycomb structures, the present paper provides a highly desired specific insight over the polaron transport mechanism in armchair graphene nanoribbons of the two most important families [28], i.e., $3p$ and $3p+1$.

The present paper is organized as follows: In Sec. II we discuss the main remarks of the model used to simulate the charge carrier dynamics in two-dimensional lattices, Sec. III contains our results as well as their analysis, and we summarize our findings in Sec. IV.

II. MODEL AND METHOD

The nature of our model follows that of the quasiparticles of which we are concerned in the present paper: It is described by a hybrid Hamiltonian with classical terms to take the phonon modes into account, quantum terms to describe the π electrons, and terms that are responsible for the coupling between the two realms. The goal is to simulate a two-dimensional "masses and springs" lattice whose π-electron clouds are connected to the displacement of the cores. We should emphasize that although this kind of approach seems to be almost naively simple, it has indeed been employed with remarkable success with the description of several different solid state systems [29,30]. Figure 1 presents the sites labeling for the honeycomb two-dimensional hexagonal lattice treated in this paper.

For such a chain, we choose to treat the vibrational modes in a harmonic approximation, which is known to be accurate in the case of nanostructures whose lattice displacement is no greater than 2%, as is the case for AGNRs. The same small displacement consideration supports the adopted approximation of expanding the π electrons hopping integrals up to first order in the displacement coordinate for the electron-phonon coupling part of the Hamiltonian. The π electrons themselves are treated with a second quantized formalism of quantum mechanics in the scope of a nearest-neighbor tight-binding approximation. The complete Hamiltonian considered, thus, takes the form:

$$H = -\sum_{\langle i,j\rangle,s}[e^{-i\gamma A_{i,j}}(t_0-\alpha y_{i,j})C^{\dagger}_{i,s}C_{j,s} + e^{i\gamma A_{i,j}}(t_0-\alpha y_{i,j})C^{\dagger}_{j,s}C_{i,s}] + \frac{1}{2}\sum_{\langle i,j\rangle}K(y_{i,j})^2+\frac{1}{2}\sum_i\frac{P_i^2}{M}. \quad (1)$$

In this expression, i and j index two arbitrary neighboring sites on the chain. $y_{i,j}$ represents the variation on the existing bond distance between two such sites. $C_{i,s}$ is the annihilation operator of a π electron with spin s in the ith site and $C^{\dagger}_{j,s}$ the corresponding creation operator at site j. t_0 is the transfer integral usually employed in pure tight-binding models. α is the electron-phonon coupling constant, which is responsible for including the interdependency between the electron and the lattice degrees of freedom.

As already mentioned, our model adopts the hopping integral as being defined by taking lattice relaxation into account. Therefore, terms such as $(t_0-\alpha y_{i,j})C^{\dagger}_{i,s}C_{j,s}$, that appear in the first sum of the Hamiltonian, describe the hopping of an electron from site j to site i, for the term under brackets represents the amplitude of probability of finding an electron originally from site j in site i. The multiplicative term $e^{-i\gamma A_{i,j}}$ ($e^{-i\gamma A_{i,j}}=e^{-i\gamma\mathbf{A}\cdot\hat{\mathbf{r}}_{i,j}}$, where $\hat{\mathbf{r}}_{i,j}$ is the unit vector pointing from site j to i) appears because we consider an external electric field by including the time-dependent vector potential $\mathbf{A}(t)$ through a Peierls substitution of the phase factor to the hopping integral [31], with $\mathbf{E}(t)=-(1/c)\dot{\mathbf{A}}(t)$. In this exponential, $\gamma\equiv ea/(\hbar c)$, a is the lattice parameter, e the absolute value of the electronic charge, and c the speed of light. The second sum of Eq. (1) is related to the effective potential associated to the σ bonds in a harmonic approximation, K being the Hooke constant. Denoting P_i as the momentum of the ith site with mass M, the third term accounts for the kinetic energy of the lattice.

The solution procedure begins by considering an initial set of coordinates $\{y_{i,j}\}$ and constructing a stationary electronic Hamiltonian from the first term of Eq. (1). The diagonalization of such Hamiltonian provides eigenvalues—E_k—and eigenvectors—$\psi_{k,s}(i,t=0)$—of the electronic part of the system for the initial time. As a result, the quantities are related as

$$E_k\psi_{k,s}(i,t=0) = -t_{i,j}\psi_{k,s}(j,t=0)-t_{i,j'}\psi_{k,s}(j',t=0) - t_{i,j''}\psi_{k,s}(j'',t=0), \quad (2)$$

where i, j, j', and j'' stand for neighboring sites.

As for the lattice, we employ the classical approach of solving the Euler-Lagrange equation. In order to do so, we evaluate the Lagrangian's expectation value $\langle\Psi|L|\Psi\rangle$, using the total wave function obtained from the diagonalization of

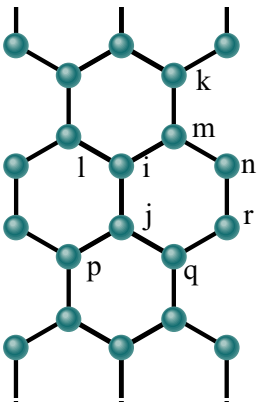

FIG. 1. Schematic labeling of an armchair GNR.

the electronic Hamiltonian. This procedure results in:

$$\langle L\rangle = \frac{1}{2}\sum_i \frac{P_i^2}{M} - \frac{1}{2}\sum_{\langle i,j\rangle} K(y_{i,j})^2 + \sum_{\langle i,j\rangle,s}[(t_0 - \alpha y_{ij})B_{i,j} + \text{c.c.}],$$

where

$$B_{i,j} \equiv \sum_{k,s}{}' e^{-i\gamma A_{i,j}} \psi^*_{k,s}(i,t)\psi_{k,s}(j,t) \tag{3}$$

is the term responsible for coupling the classical and quantum parts of our solution. Note that the prime means the sum is carried out over the occupied states only, following a Fermi-Dirac distribution function. Since a positively charged polaron has spin 1/2, we sum up to the last occupied levels, with the number of up spin levels being bigger than the number of down spin by one.

One can now make use of the calculated Lagrangian to solve the Euler-Lagrange equation under the condition $P_i = 0$. This solution will give rise to a new set of $y_{i,j}$ values; this new set can be plugged into a new electronic Hamiltonian whose diagonalization yields new wave functions and energies as in Eq. (2); these new wave functions are used to obtain yet another Lagrangian that can be used for the solution of the new Euler-Lagrange equation. The procedure is to be self-consistently performed until a given convergence criteria is achieved.

After convergence, one can say that the obtained initial state is self consistent for the degrees of freedom of both electrons and lattice. Therefore, the time evolution of this initial state can be performed according to the time dependent Schrödinger equation. By expanding the wave function $|\psi_{k,s}(t)\rangle$ in terms of $\{|\phi_{l,s}(t)\rangle\}$, a basis set of eigenstates of the electronic Hamiltonian at a given time t, the time evolved wave function from instant t to instant $t + dt$ turns out to be:

$$\begin{aligned}|\psi_{k,s}(t+dt)\rangle &= e^{-\frac{i}{\hbar}\int_t^{t+dt} dt' H(t')}|\psi_{k,s}(t)\rangle \\ &= e^{-\frac{i}{\hbar}H(t)dt}\sum_l |\phi_{l,s}(t)\rangle\langle\phi_{l,s}(t)|\psi_{k,s}(t)\rangle \\ &= \sum_l \langle\phi_{l,s}(t)|\psi_{k,s}(t)\rangle e^{-\frac{i}{\hbar}\varepsilon_l(t)dt}|\phi_{l,s}(t)\rangle,\end{aligned} \tag{4}$$

where $\varepsilon_l(t)$ denotes the eigenenergy corresponding to the eigenstate $|\phi_{l,s}(t)\rangle$.

The lattice dynamics is obtained from the solution of Eq. (4), which we compute numerically [11] and employ to the calculation of the expectation value of a new Lagrangian. Thus, the solution of the Euler-Lagrange equation is coupled with the electronic part of the system and results in the following Newtonian equation type expression for bonds with four neighboring bonds (as y_{ij} in Fig. 1):

$$F_{ij}(t) = M\ddot{y}_{ij} = \tfrac{1}{2}K[y_{il} + y_{mi} + y_{jp} + y_{qj} - 4y_{ij}] + \tfrac{1}{2}\alpha[B_{il} + B_{mi} + B_{jp} + B_{qj} - 4B_{ij} + \text{c.c.}]. \tag{5}$$

For bonds with three neighboring bonds (y_{nm} in Fig. 1) the lattice equation of motion is

$$F_{nm}(t) = M\ddot{y}_{nm} = \tfrac{1}{4}K[3y_{nr} + 2y_{km} + 2y_{mi} - 7y_{nm}] + \tfrac{1}{4}\alpha[3B_{nr} + 2B_{km} + 2B_{mi} - 7B_{nm} + \text{c.c.}]. \tag{6}$$

For bonds with just two neighboring bonds (y_{nr} in Fig. 1) the expression is

$$F_{nr}(t) = M\ddot{y}_{nr} = \tfrac{1}{4}K[3y_{nm} + 3y_{rq} - 6y_{nr}] + \tfrac{1}{4}\alpha[3B_{nm} + 3B_{rq} - 6B_{nr} + \text{c.c.}]. \tag{7}$$

It should be pointed out that ions do not necessarily react instantaneously with the electronic cloud deformation at each step. They react following their equations of motion that depend on the expectation values associated with the electronic part, at the due time. All we are doing is not to assume *a priori* that this change is negligible. We allow the equations to tell how small the changes are.

As a final remark of the model, we should dedicate a few words to the inclusion of the time dependent electric field. As we wanted our results to be a loyal manifestation of the interaction between the quasiparticles and the structural defects, we decided to include electric field adiabatically in the system. This kind of procedure avoids artificial numerical oscillations that usually appear due to an otherwise abrupt implementation of the electric field and has shown to present very good results [32]. Our adiabatical implementation of the electric field is carried out according to the time dependent scheme:

$$\mathbf{A}(t) = \begin{cases} 0 & \text{if } t < 0, \\ \frac{-1}{2}c\mathbf{E}\left[t - \frac{\tau}{\pi}\sin\left(\frac{\pi t}{\tau}\right)\right] & \text{if } 0 \leqslant t < \tau, \\ -c\mathbf{E}\left(t - \frac{\tau}{2}\right) & \text{if } \tau \leqslant t \leqslant t_f. \end{cases} \tag{8}$$

Here, t_f is the total simulation time, $t_f = 60$ fs. τ denotes the instant where electric field reaches its maximum, $\tau = 20$ fs.

The Hamiltonian of Eq. (1), as well as the method hitherto described, is completely general for the symmetry presented in Fig. 1. So far, no distinction between what is the particular species concerned has been made. In other words, this same scheme can be followed to treat any kind of two-dimensional hexagonal lattices mentioned in the introduction with additional improvements in the Hamiltonian if necessary. We have reached the point, however, to particularize our description in favor of obtaining the correct numerical values for a particular system, namely AGNR. One should bear in mind, however,

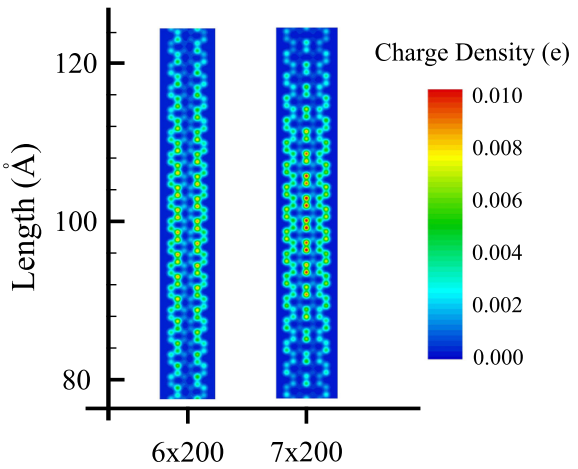

FIG. 2. Charge density distribution for 6 × 200 nanoribbon (a) and 7 × 200 nanoribbon (b) AGNRs.

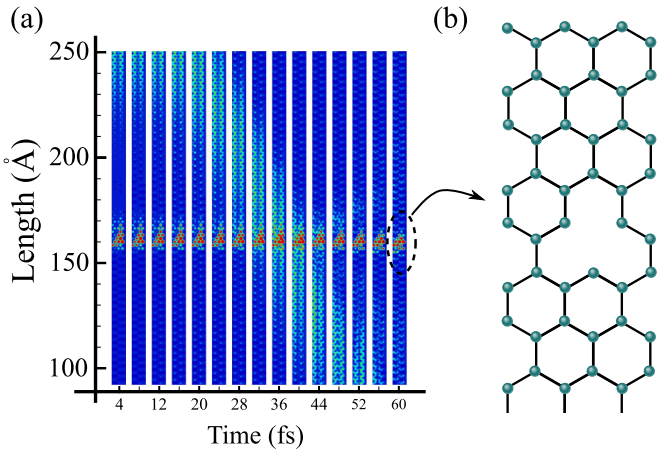

FIG. 3. Dynamics of a polaron (a) in a lattice with a vacancy positioned as in (b).

that although a certain choice of parameters is to be made to obtain the correct quantitative values for the respective kind of system, our results are expected to be qualitatively valid for the other systems as well.

The first distinction we make in favor of AGNR is to consider periodic boundary conditions in the vertical direction of Fig. 1. In this kind of system, edge effects should be mitigated in this direction, for nanoribbons consist of long lattices in their length when compared to their width. Concerning the model parameters, in our paper the values used for the constants t_0 and α were, respectively, 2.5 eV and 4.1 eV/Å [33]. We chose these values after performing preliminary simulations considering values of α that lie in the range from 3.5 to 10 eV/Å. The results show that the existence of polarons is conditioned to the presence of the electron-phonon coupling for these systems. Nevertheless, for electron-phonon constants between 4 and 6 eV/Å, the dynamics are rather insensitive to the change of this variable. According to the literature, these are suitable values for GNRs [34]. A similar analysis was carried out in terms of the harmonic elastic constant K, with $K = 21\,\mathrm{eV/Å}^2$ [33]. As M is just C core's mass, it was set up to be that of the most stable carbon isotope.

III. RESULTS AND DISCUSSION

As we have previously discussed, although our model is expected to be suitable for different two-dimensional nanolattices, we present results specifically for armchair graphene nanoribbons. In order to eliminate edge effects on the undesired direction, we consider nanoribbons of 200 sites length with periodic boundary conditions. This considerable size is important to comfortably accommodate the large polarons that usually arise in this kind of system [35]. We are mainly interested in investigating structural effects over the charge carrier transport mechanism. It is, thus, reasonable to consider the two structurally different families that are known to present polaronic transport in these materials. Therefore, results of a 6×200 nanoribbon ($3p$ family) and of a 7×200 nanoribbon ($3p + 1$ family), in which vacancies are constructed by extracting carbon atoms from different sites are presented.

Before studying the effect of the vacancy over the polaron dynamics, it is instructive to perform a characterization of the polaron from a static point of view in the two different chains without vacancies, i.e., with all the carbon atoms attached. The idea is to provide a picture of how a polaron arises in a pristine chain in order to better appreciate the effects of the vacancies in the following simulations for the two different families. Throughout the present paper, a polaron is created by extracting an electron from the highest occupied energy level. The polaron is initially positioned on the top part of the ribbon. We should stress that this is an arbitrary choice made to better present the transport picture. Since periodic boundary conditions in the nanoribbon length are considered, the only really important factor is the relative distance between the polaron and the vacancy. The initial localization of the polaron in the ribbon is obtained by moving ions slightly ($|y_{i,j}| \sim 0.01$ Å) from the equidistant position only in the upper part of the nanoribbon in the initial guess of the iteration procedure. The iterative procedure is performed until self consistency is achieved. Figure 2 presents the comparison between the charge distribution on the 6×200 [(a)] and 7×200 [(b)] nanoribbons. One can clearly see that two different patterns arise to match the symmetry of each chain. Whereas for the 6×200 nanoribbon two different centers

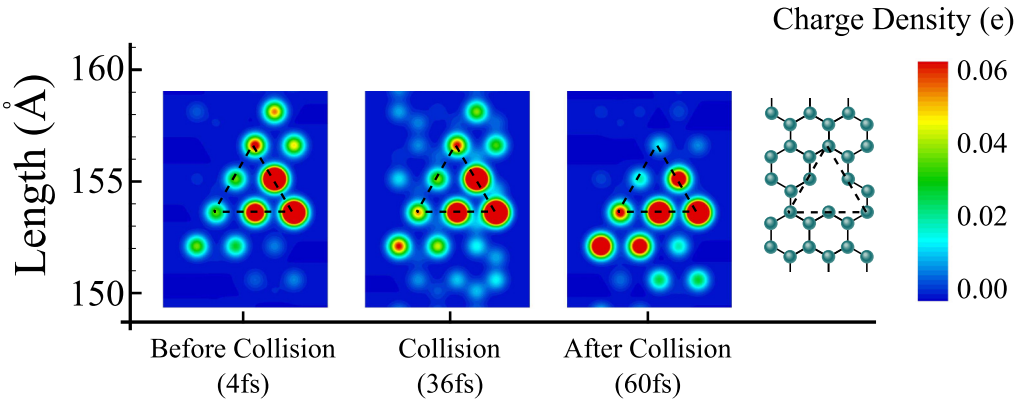

FIG. 4. Vacancy state charge density: (a) before the collision (4 fs), (b) during the collision (36 fs), and (c) after the collision (60 fs). (With a zoom in the scattering region.)

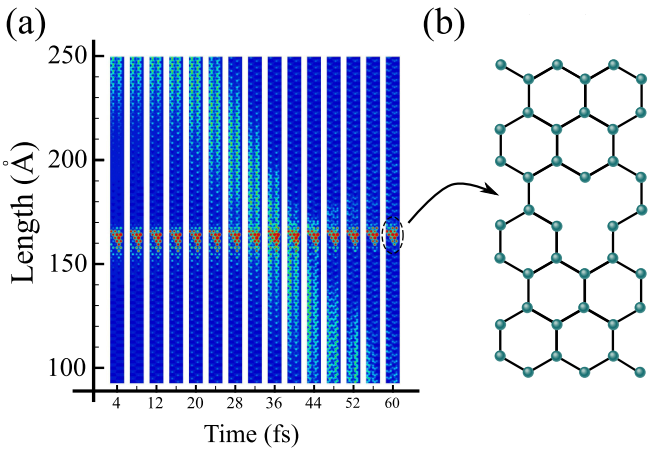

FIG. 5. Dynamics of a polaron (a) in a lattice with a vacancy positioned as in (b).

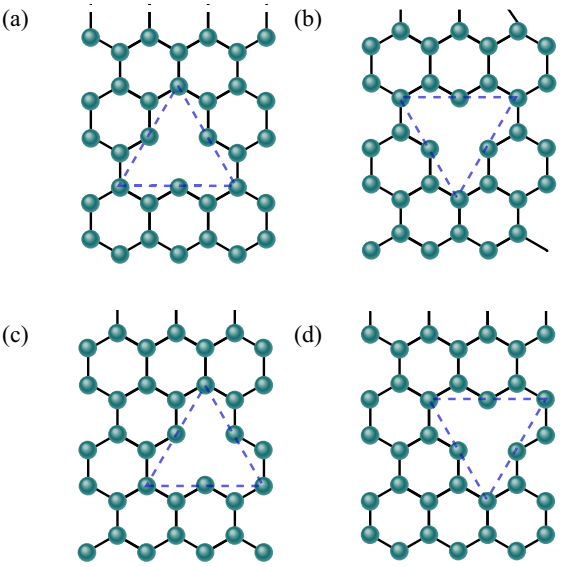

FIG. 7. Different vacancy position for 7×200 AGNR: (a) central-up, (b) central-down, (c) side-up, (d) side-down.

of charge distribution are symmetrically concentrated near the edges of the nanoribbon, the 7×200 case presents three such centers, including one exactly over the carbons that lie in the fourth column of the nanoribbon, i.e., the middle of the lattice width. This behavior of the charge distribution is a consequence of the parity of the number of sites in the nanoribbon width, and is a feature already observed in other works of the literature. Notwithstanding it is important to keep these results in mind, so that we can evaluate the impact of differently placed vacancies to be discussed in the following paragraphs.

We begin by analyzing the dynamics of the polaron in vacancy endowed 6×200 lattices. As both sides of the nanoribbon are symmetric, there are, in principle, only two different possibilities for positioning a single vacancy in the chain related to the polaron. The vacancies can be obtained as follows: We either extract one carbon from sublattice A (we call this the *up* configuration) or we extract one carbon from sublattice B (similarly, we call this the *down* configuration). A graphical representation of the *up* and *down* configurations of vacancies is presented in Figs. 3(b) and 5(b), respectively. Figures 3(a) and 5(a), to be discussed in the following, consist on the time evolution of the polaron position in chains with vacancies positioned according the two different configurations. The polaron movement results from the application of a 0.065 mV/Å electric field oriented to move the quasiparticle directly towards the vacancy. One should note that the change of slope that is clearly observed in the trajectory of the polaron from the initial time steps towards the rest of the simulation is due to the adiabatical application of the electric field. After the transient expressed by 8, the value of 0.065 mV/Å is maintained.

Figure 3(a) presents the case of an *up* vacancy. The first thing we notice is the difference between the charge distribution at the initial instant here with that of Fig. 2(a), i.e., the case without vacancy. One can clearly see that, although the same pattern of charge distributed in two centers along symmetrically displaced columns arises, the vacancy concentrates charge around itself so that we can no longer observe the symmetrical distribution along the length of the nanoribbon. Similar results are obtained for other defects such as impurities, and they are to be attributed to a natural

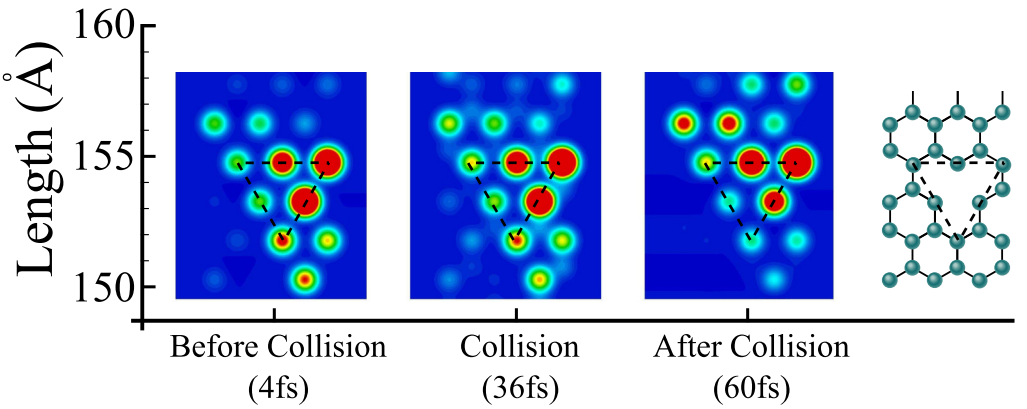

FIG. 6. Vacancy state charge density: (a) before the collision, (b) during the collision, and (c) after the collision. (With a zoom in the scattering region.)

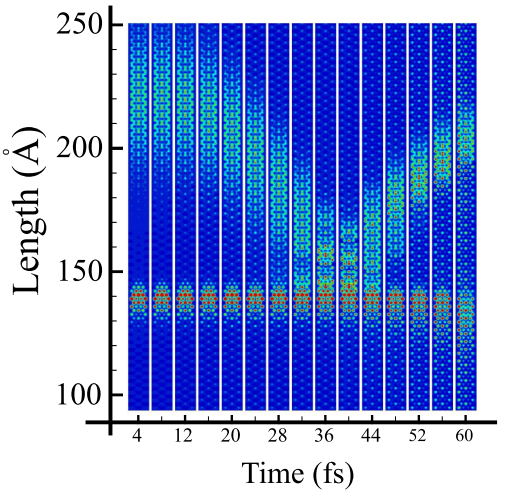

FIG. 8. Dynamics of a polaron in a 7×200 lattice with a central-up vacancy [positioned as in Fig. 7(a)].

symmetry breaking both impurities or vacancies cause in the lattice. Next, we gather our attention to the movement of the polaron itself. As the electron field accelerates the polaron towards the defect, we can see that some of its charge is spread throughout the lattice. Also, we can note that some of the polaron's charge is imprisoned by the sites around the vacancy. This partial charge trapping is easily observed when the actual collision takes place, i.e., when the polaron moves over the vacancy. One can observe that even after that instant, the defect remains with accumulated charge but it gradually releases some of it as the electric fields continue to act.

We have thus seen that the movement of the polaron over the vacancy changes its charge distribution. In order to have a more accurate view of how this change takes place, we present in Fig. 4 a series of snapshots focused in the region of the collision at three instants: before the collision (4 fs), at the collision (36 fs), and after the collision (60 fs). The change of the charge distribution on the region of the vacancy is pretty clear. Also we can conclude that its surroundings end up being slightly more charged with the scattering process, the excess charge originally coming from the polaron. In other words, the polaron delocalization is closely related to a certain degree of charge trapping by the vacancy. We should emphasize that this charge redistribution around the vacancy is a general effect. Indeed, a clear indication of this fact can be appreciated by considering that a similar phenomena takes place in vacancy endowed graphene sheets, as recently reported in the literature [36]. This redistribution of charge density actually is also the kind of process that explains the features described by Scuzeria [20] as far as the gas adsorption properties are concerned.

Figure 5(a) presents the case of a vacancy positioned according to the second configuration (*down* configuration). The most important feature concerning Fig. 5(a) is that it is identical to the one obtained for the *up* configuration, i.e., Fig. 3(a). As expected, this should indeed be the case. Because of the symmetry of this even nanoribbon, the extraction of a carbon atom makes the vacancy state occupy the whole width of the ribbon. Added to this is the fact that the difference between the configurations *up* and *down* is merely that one is upside down in relation to the other, so that the polaron faces the exact same potential barrier when it reaches the point of crossing the defect, the difference being the orientation of the potential barrier.

To confirm this point we present, in Fig. 6, the snapshots before, during, and after the collision represented by Fig. 5. One can readily see that the pattern observed in Fig. 6 is nothing but an inverted version of what is seen in Fig. 4, thus confirming what was said about the invariance of the polaron interaction with the differently positioned vacancies. In other words we can conclude that for an AGNR of even width, provided the vacancy state is spread over its width center, its position does not play an important role over the behavior of the polaron's dynamics. As this property arises from symmetry considerations, it is clear that this result is valid for other two-dimensional lattices of the same symmetry as well.

A completely different pattern is found for the more complex case of an odd width nanoribbon, as is the case of the 7×200 member of the $3p + 1$ family, to be henceforward discussed. To begin with, in this case we observe that there are not two but four potentially different positions to create a vacancy related to the polaron. Figure 7 present the different possibilities. Our notation here is a generalization that follows from the one adopted in the previous paragraph: The vacancy depicted in Fig. 7(a) is called central-*up*; in 7(b) we have a central-*down* vacancy. 7(c) is described as a side-*up* defect, and 7(d) is the side-*down* case. Symmetry arguments allow us to assess conclusively that no distinction is to be made of the side from which the carbon is extracted. Also, following the same arguments discussed in the previous paragraph we

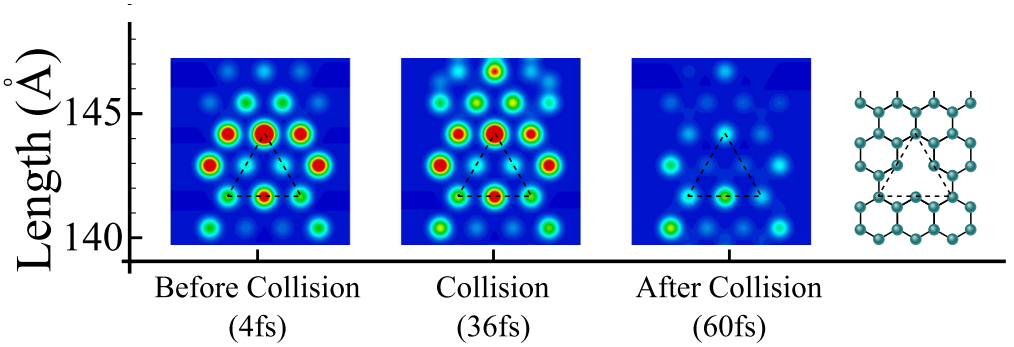

FIG. 9. Before (4 fs), during (36 fs), and after the collision (60 fs): a zoom in the scattering region.

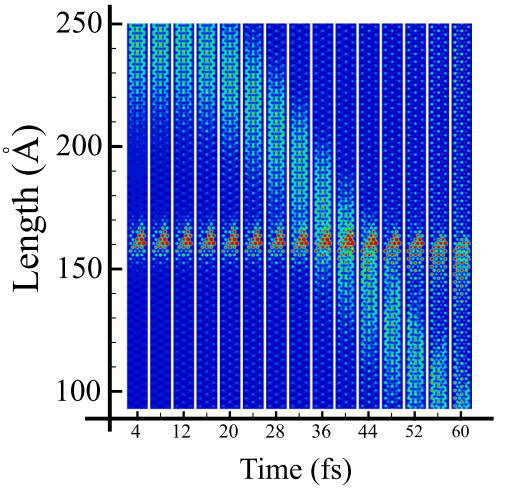

FIG. 10. Dynamics of a polaron in a 7 × 200 lattice with a side-up vacancy [positioned as in Fig. 7 (c)].

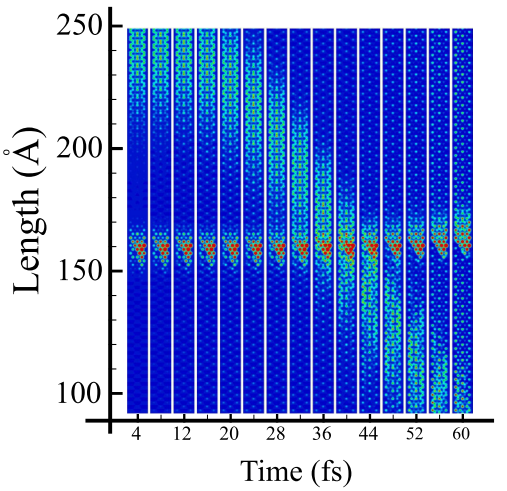

FIG. 12. Dynamics of a polaron in a 7 × 200 lattice with a side-down vacancy [positioned as in Fig. 7(d)].

can readily rule out the possibility of (a) and (b) presenting qualitative different results whatsoever. Again, what we have is a symmetrically displaced vacancy that is perceived by the polaron in the same way. Note that both (a) and (b), which are positioned in the center of the ribbon, make their surrounding likely, so that we have the same response as observed in the case of 6 × 200 concerning the difference between *up* and *down* configurations. Naturally, we do not expect the results from 6 × 200 to be in any way similar to the ones from 7 × 200, as the family and the size of the nanoribbon are known to play an important role over the quasiparticle transport. As for (c) and (d), although one can see that they too differ by i symmetry operation, the vacancy state does not occupy the lattice width symmetrically. The difference between these latter situations can be understood by imagining the polaron flowing in opposite directions in one of the cases. The effective potential barrier it must surpass is, in principle, expected to be different, because the space is occupied differently. Therefore one has no reason to expect the same results.

Figure 8 depicts the dynamics of a polaron in a 7 × 200 lattice in which a central-*up* vacancy is considered, i.e., a defect represented by Fig. 7(a). A somewhat different scattering mechanism takes place in this case. Again the polaron is accelerated directly towards the vacancy, and the electric field provides some extra delocalization to the quasiparticle, as can be observed from the increasing spreading of its charge. However, this time the polaron is not able to pass directly through the defect but rather bounces back to the original direction. The similar absolute value of the slope of the polaron's trajectory around the scattering region suggests that an almost elastic collision took place. Interestingly, in doing so, it extracts some of the charge that was concentrated around the defect and ends up being slightly more charged, as can be seen from the more reddish pattern that appears over its structure. It should be pointed out that the electric field is still in the same direction and acts on the polaron decelerating it. This can be seen by the curve it makes after the collision. The point is that, differently from the previous case, the polaron did not pass through the vacancy in the first interaction between the structures. Even if it is for the polaron eventually surpassing this potential barrier due to fluctuations, one can clearly see that the overall system's charge mobility in this case is much smaller than in the previous case.

This later effect can be better visualized by focusing on the vacancy region and analyzing its charge distribution before, during, and after the collision. From Fig. 9 one can clearly see that a considerable amount of the charge that was initially over the vacancy region vanishes from it after the polaron's

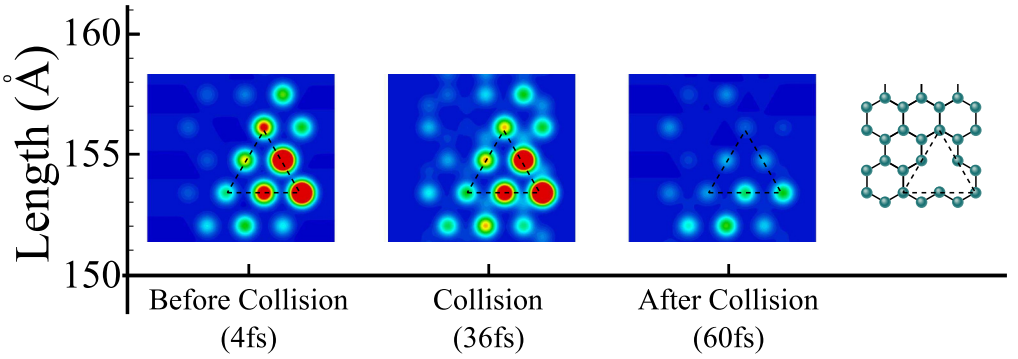

FIG. 11. Before, during, and after the collision: a zoom in the scattering region.

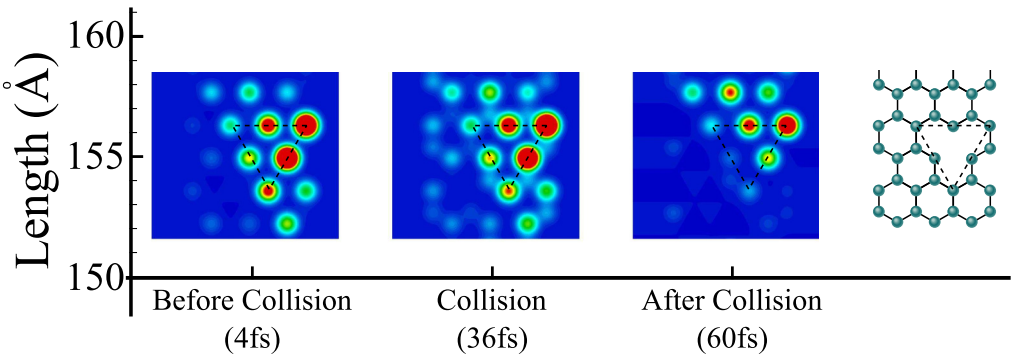

FIG. 13. Before, during, and after the collision: a zoom in the scattering region.

collision. Although some of the lost charge is simply spread over the lattice, a considerable amount is coupled by the polaron that, as it turns out, is responsible for the decrease of charge of the defect. The results here discussed are of fundamental importance, particularly when taking those of the 6×200 case into consideration. Particularly, symmetry arguments allow us to trace a parallel between the structures from Fig. 7(a) and those of Fig. 3(b). However, the respective results of Figs. 8 and 3(a) strongly differ. This is important evidence that, no matter how similar are the defects, the family of the nanoribbon (and its size, thereof) plays an important role on the transport mechanism of polarons, and how they interact with vacancies. Here we have an example of the kind of process that explains Stafström's [23] conclusion concerning the loss of conductivity nanostructures may present when vacancies are considered.

We now move further to the interesting cases of lateral defects, beginning with the so-called side-up vacancy of Fig. 7(c), whose dynamics is presented in Fig. 10. One can clearly see that, for this simulation, the polaron was able to pass through the vacancy. A comparison between the results from the currently analyzed simulations with those of Fig. 8 shows that, indeed, the positioning of the vacancy is of fundamental importance to the transport mechanism of the polaron. For instance, the fact that this configuration allowed for a transmission of the polaron through the lattice suggests that this kind of vacancy results in a system in which the quasiparticle has more mobility, which ultimately may affect the conductivity of the system.

In the process of passing through the vacancy, we can see that, again, the emerging polaron is more charged than before the collision. Figure 11 presents the snapshots concentrated in the vacancy region. After the collision, the diminishing of the charge concentrated in the vacancy is quite clear. Again, the simulation suggests a quasielastic collision. Note the similarity between the charge distribution before and during the collision. From that we conclude that the polaron drags some of the vacancy charge as it moves away from the defect after the scattering process.

We are in the point of presenting the final system considered in the present paper: the 7×200 AGNR with a side-down type vacancy according to Fig. 7(d). Figure 12 depicts a very similar pattern for this case. The analysis of the region around the defect presented in Fig. 13 shows an analogous behavior for the vacancy state after the collision.

In order to provide a clearer visualization of the process, we present, in Fig. 14, a 3D representation of the polaron dynamics over the AGNR with the side-*down* vacancy. The nanoribbon lies in the xy plane, whereas the z height is a measure of the charge density at that point. After the collision, we can see a charge scattering around the vacancy. In fact, comparing the charge density before the collision, the charge spreads over a larger region. This can readily be seen from the more uniform size of the peaks after the collision.

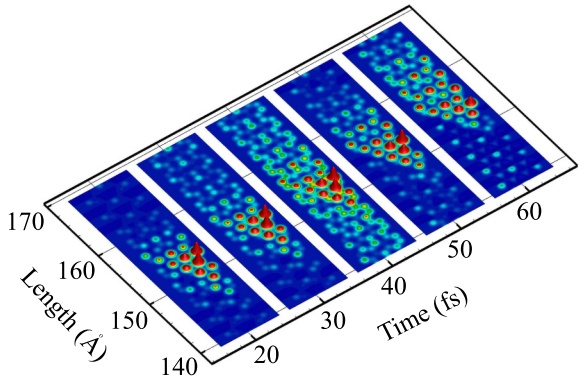

FIG. 14. 3D representation of the charge density associated with the vacancy state.

IV. CONCLUSIONS

In summary, we have developed a model to describe charge transport on two-dimensional honeycomb hexagonal lattice nanostructures in the presence of vacancy defects. Specifically we parametrize our model to describe narrow AGNRs of the two semiconducting families ($3p$ and $3p + 1$). We observe that, in general, the position of the vacancy on the lattice is fundamental to define the kind of scattering process of the polaron by the vacancy. As expected, the width of the nanoribbon is also important in defining the behavior of the system. We found that the parity of the width and vacancy positions can have such critical importance that their effects span from allowing a polaron to freely move through the lattice to being reflected by the collision with the vacancy.

They also control the trapping and releasing of charge process between the quasiparticle and the vacancy, thus defining the structure that ends up being more charged after the scattering process. As we have seen that both the dynamical scattering process (including the behavior of the arising charge carrier) and the charge distribution of the system is differently affected depending on structural properties of the system, the generality of our model allows us to provide a qualitatively important description on how these effects might play a role over the performance of systems based on several different two-dimensional nanostructures. As an example—as is the case of the AGNRs results that we have discussed—our approach can be used to predict whether a higher or lower conductivity is to be expected depending on the kind of defects present, therefore being of major interest to the molecular electronics community.

ACKNOWLEDGMENTS

The authors gratefully acknowledge the financial support from the brazilian research councils CAPES, CNPq, and FINATEC. The present work started when one of the authors (G.M. e Silva) was visiting Osaka City University, Japan. He appreciates the financial support from the Osaka City University.

[1] E. Bundgaard and F. C. Krebs, Sol. Energ. Mat. Sol. **91**, 954 (2007).
[2] J. Zhao, A. Buldum, J. Han, and J. P. Lu, Nanotechnology **13**, 195 (2002).
[3] A. Soltani, S. G. Raz, V. J. Rezaei, A. D. Khalaji, and D. Savar, Appl. Surf. Sci. **263**, 619 (2012).
[4] L. M. Xie, Nanoscale **7**, 18392 (2015).
[5] J. Singleton and C. Mielke, Contemp. Phys. **43**, 63 (2002).
[6] M. Y. Han, B. Ozyilmaz, Y. Zhang, and P. Kim, Phys. Rev. Lett. **98**, 206805 (2007).
[7] V. Coropceanu, J. Cornil, D. A. da Silva Filho, Y. Olivier, R. Silbey, and J.-L. Bredas, Chem. Rev. **107**, 926 (2007).
[8] C. Kittel, *Introduction to Solid State Physics*, 8th ed. (Wiley, New York, 2004).
[9] J-L Bredas and G. B. Street, Acc. Chem. Res. **18**, 309 (1985).
[10] G. M. e Silva, Phys. Rev. B **61**, 10777 (2000).
[11] M. P. Lima and G. M. e Silva, Phys. Rev. B **74**, 224304 (2006).
[12] P. H. de Oliveira Neto, W. F. da Cunha, R. Gargano, and G. M. e Silva, J. Phys. Chem. A **113**, 14975 (2009).
[13] W. F. da Cunha, L. F. Ribeiro Junior, A. L. A. Fonseca, and G. M. e Silva, J. Phys. Chem. C **118**, 23451 (2014).
[14] S. Okuno and Y. Onodera, J. Phys. Soc. Jpn. **52**, 3495 (1983).
[15] L. F. Ribeiro Junior, W. F. da Cunha, P. H. de Oliveira Neto, R. Gargano, and G. M. e Silva, J. Phys. Chem. B **117**, 11801 (2013).
[16] D. Zhao, Q. Huo, N. Melosh, G. H. Frederickson, B. F. Chmelka, and G. D. Stucky, Science **279**, 548 (1998).
[17] K. S. Kim, Y. Zhao, H. Jang, S. Y. Lee, J. M. Kim, K. S. Kim, J. H. Ahn, P. Kim, J. Y. Choi, and B. H. Hong, Nature (London) **457**, 706 (2009).
[18] H. W. Wang, K. Kalandar-Zadeh, A. Kis, J. N. Coleman, and M. S. Strano, Nat. Nanotechnol. **7**, 699 (2012).
[19] P. Ruffieux, S. Wang, B. Yang, C. Sánchez-Sánchez, J. Liu, T. Dienel, L. Talirz, P. Shinde, C. A. Pignedoli, D. Passerone, T. Dumslaff, X. L. Feng, K. Mllen, and Roman Fasel, Nature (London) **531**, 489 (2016).
[20] H. F. Bettinger, T. Dumitrica, G. E. Scuseria, and B. I. Yakobson, Phys. Rev. B **65**, 041406 (2002).
[21] P. Piquini, R. J. Baierle, T. M. Schmidt, and A. Fazzio, Nanotechnology **16**, 827 (2005).
[22] X. M. Li, W. Q. Tian, X. R. Huang, C. C. Sun, and L. Jiang, J. Nanopart. Res. **11**, 395 (2009).
[23] A. Hansson, M. Paulsson, and S. Stafström, Phys. Rev. B **62**, 7639 (2000).
[24] W. F. da Cunha, L. F. Ribeiro Junior, A. L. A. Fonseca, R. Gargano, and G. M. e Silva, Carbon **91**, 171 (2015).
[25] A. Dimiev, D. Zakhidov, B. Genorio, K. Oladimeji, B. Crowgey, L. Kempel, E. J. Rothwell, and J. M. Tour, ACS Appl. Mater. Interfaces **5**, 7567 (2013).
[26] L. Li, A-R. O. Raji, and J. M. Tour, Adv. Mat. **25**, 6298 (2013).
[27] L. Li, A-R O. Raji, H. Fei, Y. Yang, E. L. G. Samuel, and J. M. Tour, ACS Appl. Mater. Interfaces **5**, 6622 (2013).
[28] Y. W. Son, M. L. Cohen, and S. G. Louie, Phys. Rev. Lett. **97**, 216803 (2006).
[29] W. F. da Cunha, L. F. Ribeiro Junior, R. Gargano, and G. M. e Silva, Phys. Chem. Chem. Phys. **16**, 17072 (2014).
[30] L. F. Ribeiro Junior, E. F. da Cunha, A. L. A. Fonseca, and G. M. e Silva, J. Phys. Chem. Lett. **6**, 510 (2015).
[31] Y. Ono and A. Terai, J. Phys. Soc. Jpn. **59**, 2893 (1990).
[32] M. Kuwabara, Y. Ono, and A. Terai, J. Phys. Soc. Jpn. **60**, 1286 (1991).
[33] V. N. Kotov, B. Uchoa, V. M. Pereira, F. Guinea, and A. H. Castro Neto, Rev. Mod. Phys. **84**, 1067 (2012).
[34] J. Yan, Y. Zhang, P. Kim, and A. Pinczuk, Phys. Rev. Lett. **98**, 166802 (2007).
[35] P. H. de Oliveira Neto, J. F. Teixeira, W. F. da Cunha, R. Gargano, and G. M. e Silva, J. Phys. Chem. Lett. **3**, 3039 (2012).
[36] V. M. Pereira, J. M. B. Lopes dos Santos, and A. H. Castro Neto, Phys. Rev. B **77**, 115109 (2008).